SiliconPV 2023, 13th International Conference on Crystalline Silicon Photovoltaics

Silicon Solar Cell Process Technologies (Advanced Light Management, Junction Formation, Cleaning, Surface Passivation)

https://doi.org/10.52825/siliconpv.v1i.943

Published: 22 Feb. 2024

Practical J_{sc} Limits for SHJ Devices: Insights From Modelling

Erik M. Spaans[1][https://orcid.org/0000-0003-2208-368X], Selvaraj Venkataraj[1][https://orcid.org/0000-0002-4329-9319], Armin G. Aberle[1][https://orcid.org/0000-0003-0456-2070], and Nitin Nampalli[1][https://orcid.org/0000-0003-3742-1864]

[1]Solar Energy Research Institute of Singapore, National University of Singapore, Singapore

Abstract. Modern industrial silicon heterojunction (SHJ) solar cells are increasingly limited by the short-circuit current density (J_{sc}) and there is a strong interest in understanding how much novel approaches such as window layers, novel transparent conductive oxides (TCOs) and anti-reflection coatings (ARCs) could improve the J_{sc} of SHJ solar cells. In this work, the practical J_{sc} limits of SHJ solar cells are determined using a carefully calibrated ray-tracing model, validated using empirical data from in-house solar cells as well as recently published high-efficiency front-and-back contacted (FAB) SHJ solar cells. The model is then further refined to obtain a detailed J_{sc} loss breakdown of the latest record efficiency FAB SHJ solar cells, for which there are no published J_{sc} loss breakdowns. Notable advances made in these advanced solar cells with regards to window layers, TCOs and ARCs at the cell level are analysed. Based on the magnitude of impact on the solar cell J_{sc}, the most critical factors for achieving high-J_{sc} SHJ solar cells are identified and ranked. Allowing for additional improvements and combining the best approaches identified, an estimate of the practical upper limit of J_{sc} for FAB SHJ solar cells is determined to be 41.81 mA/cm^2. This work serves as a useful reference for the current state of play for J_{sc} improvements in SHJ solar cells and highlights practical pathways and issues for improving commercial SHJ solar cells.

Keywords: Silicon Heterojunction, Solar Cell, Short-Circuit Current Density, Ray Tracing, Modelling.

1 Introduction

The years 2019-2022 were an active period of development for industrial front-and-back contacted (FAB), large-area silicon heterojunction (SHJ) solar cells, with cell efficiency records being broken in rapid succession and reaching 26.81% in late 2022 [1]. Efficiency gains in recent records were largely due to J_{sc} and fill factor (FF) improvements. In particular, enablers for improved J_{sc} are the main distinguishing factor for the recent records, with nano-/microcrystalline silicon (or silicon-compound) doped layers, novel TCOs (transparent conductive oxides) and ARCs (anti-reflection coatings) being actively employed to improve the J_{sc} to as much as ~41.5 mA/cm^2 for FAB SHJ solar cells [1], as shown in Figure 1. Interestingly, however, not all high-J_{sc} record solar cells appear to utilize all available enablers, and the question of what exactly the ultimate J_{sc} limit of a FAB SHJ cell is remains open.

In this work, we focus on using modelling to derive key practical insights and quantify J_{sc} gains from these various innovative approaches, with the goal of arriving at a practical upper limit of J_{sc} for FAB SHJ solar cells utilizing demonstrable state-of-the-art technologies to improve J_{sc}.

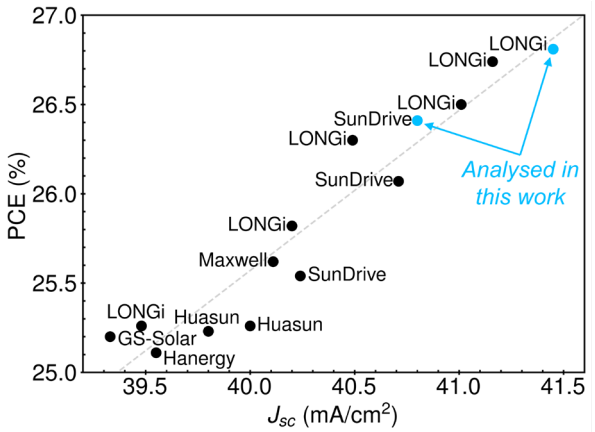

Figure 1. Certified power conversion efficiencies (PCEs) of > 25% of commercial FAB SHJ solar cells vs J_{sc} from the past years [2-15].

2 Modelling of FAB SHJ solar cells

2.1 Development of baseline optical model

An in-house fabricated SHJ solar cell was used to create a reference optical model of a SHJ device (PCE = 22.0%, J_{sc} = 37.7 mA/cm^2), the structure of which is shown in Figure 2. This was done using GenPro4 [16], a ray tracing software that combines ray and wave optics for incoherent and coherent layers, respectively. The model was calibrated by matching modelled and measured reflectance and transmittance (RT) spectra. Complex refractive indices of various functional layers were also used as a key input to the model.

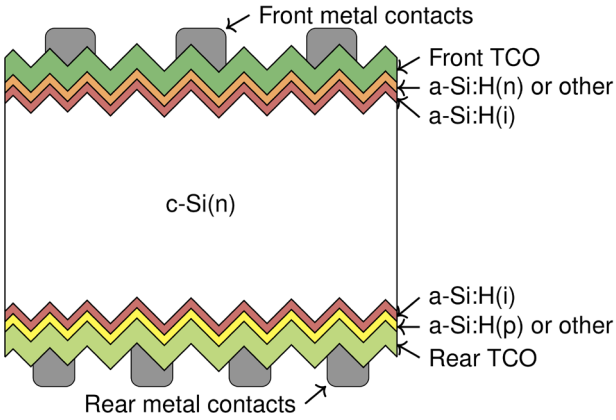

Figure 2. Cross-sectional schematic structure of the simulated FAB SHJ solar cell.

When calibrating the reference optical model, a mismatch between the measured and modelled RT spectra for solar cells can be cumbersome to correct since isolating the layer(s) causing the mismatch can be very difficult. This is because in a SHJ solar cell, there are 7-8 functional layers, each with their own complex refractive index and thickness, which give rise to the final observed RT spectra. In this work, we have addressed this issue by creating several test structures at each intermediate step of the solar cell fabrication. In each case, the RT spectra of the precursor is measured from the front and rear side and is used to calibrate the optical model.

To obtain the final J_{sc} of the device, a 100% collection efficiency (CE) for the c-Si(n), and 32% CE for the front a-Si:H(i) layer were assumed to ensure a good match to external quantum efficiency (EQE) measurements. A very similar approach was adopted by Holman *et al.* [17]. The final model for the in-house cells overestimates the integrated EQE J_{sc} by 0.55 mA/cm^2,

which we believe is due to the c-Si(n) wafer having less than 100% CE in our devices. For the record SHJ solar cells modelled in this work, a 100% CE is assumed and was found to result in a better fit to the reported EQE data. To ensure fidelity to EQE measurement conditions, a rear stack of air/Cu is added to simulate a rear chuck. Finally, since a 1D optical model is used, the effect of metal shading is factored in by reducing the (non-shaded) simulated J_{sc} by an effective shading fraction that takes into account the metallization fraction as well as the optical shading fraction for individual fingers.

2.2 Modelling of recent certified records

Here, the details regarding how the recent record SHJ FAB solar cells were optically modelled are explained. We start by calibrating models to published data from recent records of SunDrive [11] and LONGi [18]. It is important to note that the published J_{sc} data that were modelled in these works are not from the record solar cells made by the respective groups. Rather, a cell with a lower J_{sc} than the record solar cell was modelled. In order to validate our model, these lower-J_{sc} cells are modelled first to ensure an accurate match to the published loss analysis in Refs. [11] and [18]. After this, further adjustments are made to the model to achieve the best possible match to the EQE data from the record solar cells from the two groups. Using these calibrated models as a baseline, we estimate the J_{sc} loss contributions from the various functional layers, allowing a side-by-side comparison of these record devices for the first time.

For in-house fabricated layers, the complex refractive indices of the individual layers (a-Si:H(i), a-Si:H(n), a-Si:H(p), front TCO and rear TCO) were measured in-house using spectroscopic ellipsometry performed on thin films deposited on glass followed by curing at 200 °C for 10 min (same conditions as the metal curing process used during device fabrication). To estimate the refractive index of other materials (more transparent a-Si:H(i), nc-SiO_x:H(n), nc-Si:H(p) and other TCOs), complex refractive index data reported in the literature was used. It was assumed that the reported refractive index data from literature matches the layer properties in the final device. However, in certain cases where a match to the reported EQE / J_{sc} (for record solar cell data) could not be obtained using the reported refractive index data, minor adjustments were applied to the extinction coefficient (*k*) data from the literature to ensure a reasonable fit to the published EQE and reflectance data. The final complex refractive index (*n* and *k* values) for all layers used in the models shown in Figure 3 can be found in Appendix A.

2.2.1 SunDrive: from 40.24 to 40.80 mA/cm^2

To begin, the 25.54%-efficient SHJ solar cell with J_{sc} = 40.24 mA/cm^2 [11] is calibrated first. Information regarding layer thicknesses as described in Ref. [11] and reference complex refractive indices found in the literature [19-22] and measured in-house are used as starting inputs. A thickness variation of up to ±4 nm from the published thickness data in Ref. [11] is allowed in our model for each layer, allowing for spectrally resolved losses for the layers to be approximated as closely as possible. Within these constraints, it was found that the parasitic absorption of the reported device in Ref. [11] could not be fitted using only literature reported refractive index data. This is not surprising, since Ref. [11] claims several improvements were made to the thin film layers comprising the device, which resulted in significantly lower parasitic absorption. Since no refractive index data for individual layers was published in Ref. [11], it was attempted to adjust the refractive index data in order to achieve a good fit to the reported EQE and reflectance.

The reported EQE and reflectance data suggested a significantly lower parasitic absorption compared to the output of the model where the refractive index of layers was not adjusted. However, the reflectance losses in the device could be sufficiently well-modelled using the non-adjusted refractive index data. Hence, only the extinction coefficient (*k*) of certain layers was adjusted, keeping the real refractive index (*n*) the same. In the absence of raw *n*

and *k* data for all layers used in the device, this approach represents a reasonable approximation of the layer properties.

The low parasitic absorption indicated by the EQE and reflectance data in Ref. [11] could only be obtained by scaling the *k* values of the front-side nc-SiO_x:H(n) and TCO layers by a factor compared to the *k* values in the literature (see Appendix B). No adjustment was required for the refractive index of the a-Si:H(i). Finally, a 2% shading is assumed, which agrees with the reported metal finger dimensions. The resulting model was found to result in an excellent fit to the reported J_{sc} as well as the reported loss breakdown published in Ref. [11].

Next, the record solar cell from SunDrive [9] (J_{sc} = 40.80 mA/cm^2, not analysed in Ref. [11]) was modelled. The various reported innovations implemented in SunDrive's highest-efficiency SHJ solar cell [9] were taken into account. First, the shading fraction was reduced from 2% to 1.5%, as deduced from the new finger dimensions [23]. Second, a MgF_2 ARC is added on top of the front TCO to reduce reflection losses. Finally, the same transparent TCO that was used at the front side of the 40.24 mA/cm^2 cell was also introduced to the rear side, boosting the near-infrared (NIR) response of the solar cell. All in all, the final device J_{sc} for the 40.80 mA/cm^2 solar cell [9] was able to be modelled to an accuracy of within ±0.01 mA/cm^2, as seen in Figure 3.

2.2.2 LONGi: from 41.22 to 41.45 mA/cm^2

Here, the model of a SHJ solar cell with an efficiency of 26.74% and J_{sc} = 41.22 mA/cm^2 [18] is calibrated first. We assume a state-of-the-art pyramidal texturing, with a weighted average reflectance (WAR) of 12.9% in the 300-1200 nm range. A similar modelling approach as explained in Section 2.2.1 is used, where the front layers were even more transparent than in the modelled 40.80 mA/cm^2 solar cell.

In modelling the 41.22 mA/cm^2 solar cell, there was a mismatch in the NIR response of the solar cell, which resulted in a J_{sc} of about 0.2 mA/cm^2 higher. Changes to the model to correct for this deviation were evaluated, such as reducing the texturing, changing the *n* of the front TCO, varying the material of the back reflector, and reducing the wafer thickness. Some changes effectively reduced the c-Si absorption in the NIR, such as adjusting the wafer thickness. Nevertheless, these changes deviated significantly from the reported structure of the device, so they were not implemented. Instead, given that the 41.22 mA/cm^2 solar cell and LONGi's record 41.45 mA/cm^2 solar cell differ only in their NIR response, we assume our model to represent the 41.45 mA/cm^2 cell, for which no J_{sc} loss decomposition is available. The simulated EQE resulted in an excellent fit to the reported EQE in Ref. [1]. Here, a 2.1% shading is assumed, which is the same as for the 41.22 mA/cm^2 solar cell, as estimated from Refs. [1, 18]. The device J_{sc} was modelled to an accuracy of within ±0.04 mA/cm^2, as shown in Figure 3.

2.3 Practical J_{sc} limit

Here, all the high-efficiency strategies are combined to arrive at an estimation of the practical J_{sc} limit of FAB SHJ solar cells. The lowest shading fraction, estimated at 1.5%, is used in combination with the ultra-transparent layers from Ref. [18]. Finally, the thickness of the ARC is adjusted to minimize front reflectance, giving a final J_{sc} of 41.81 mA/cm^2.

3 Insights from J_{sc} modelling

3.1 Loss analysis for recent record solar cells

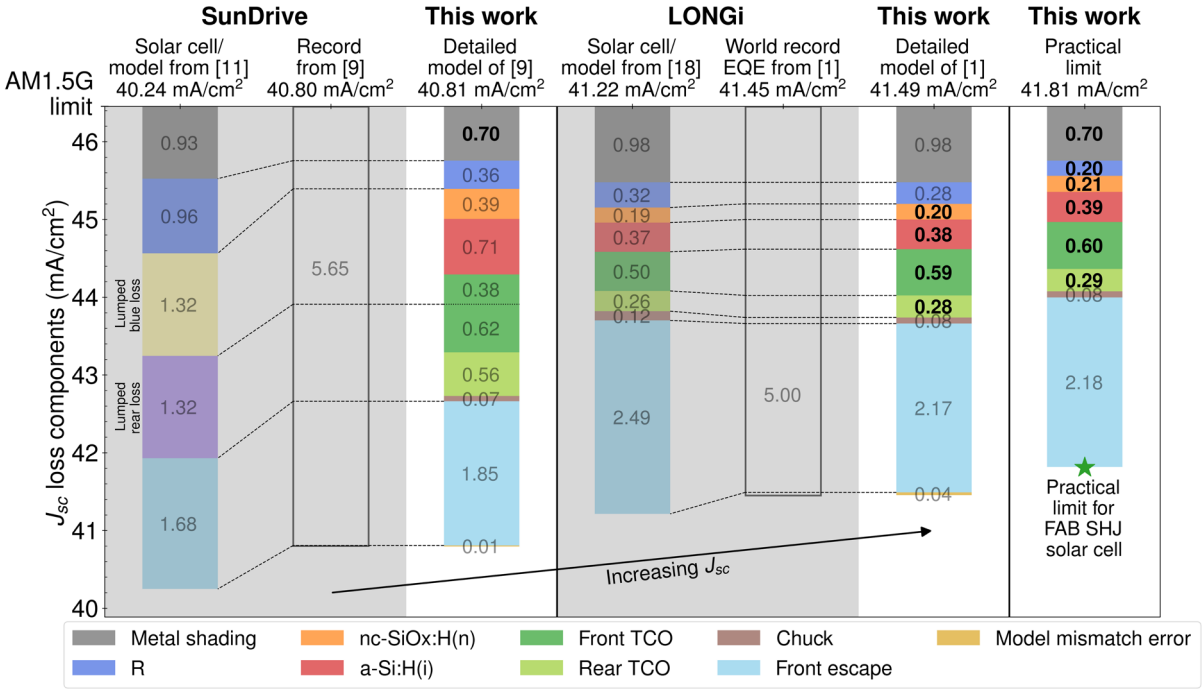

Figure 3. Detailed J_{sc} loss analysis of the latest FAB SHJ commercial record cells and practical J_{sc} limit.

The detailed J_{sc} loss breakdown of the modelled record solar cells reported in Section 2 are shown in Figure 3. The device J_{sc} increases from left to right. It can be seen that the originally published model from SunDrive for the 40.24 mA/cm^2 cell [11] (extreme left of Figure 3) has J_{sc} losses lumped in to "blue" and "rear" losses. In contrast, the more detailed model in this work further decomposes these lumped losses into contributions from all of the individual layers for SunDrive's record device (40.80 mA/cm^2 [9]). The main innovation seen here is the ultra-low shading fraction, made possible due to < 10 μm wide and high-aspect ratio Cu-plated fingers [23]. Moreover, the use of IMO (M=TiO_2+CeO_2+Ta_2O_5) [11] as TCO and nc-SiO_x:H(n) as the front-side n-type charge extraction layer improves the overall transparency of the device.

Moving on to the world-record solar cell from LONGi (41.45 mA/cm^2 [1]), the main innovations in this device are the use of indium-doped cerium oxide (ICO) as the front and rear TCO [18], greatly reducing front-side absorption in the solar cell. Moreover, the transparency of the a-Si:H(i) and nc-SiO_x:H(n) in the LONGi solar cells is remarkably high, resulting in a very low parasitic absorption. Combining all these innovations and adjusting the thickness of the ARC, we arrive at the practical J_{sc} limit for FAB SHJ solar cells of 41.81 mA/cm^2, with J_{sc} losses decomposed as shown in the extreme right bar of Figure 3.

We note that the extinction coefficient used in the models in this work were significantly lower than the values published in the literature [19-22], suggesting that significant improvements have been made to the optical properties of the thin film layers used in the record solar cells. In the absence of published refractive index data for layers present in these record solar cell devices, the adjusted refractive index data used in the models (see Appendix A and B) represent a reasonable estimate for optical modelling purposes (as indicated by the good match between modelled and published EQE and reflectance data). However, the authenticity

of the refractive index data used in our models has not been verified and may not reflect the true *n* and *k* of the layers present in the record solar cell devices.

3.2 J_{sc} improvement pathways for classic SHJ solar cells

Based on the insights above from the record high-J_{sc} FAB SHJ solar cells, a practical roadmap to achieving high J_{sc} can be charted. The starting point here is a "classic" SHJ solar cell with a J_{sc} of ~37.7 mA/cm^2, which utilizes only a-Si:H based functional layers, ITO as TCO, and 45 µm wide screen-printed metal fingers with a shading fraction of ~3.5%. The difference in J_{sc} between such a cell and the above-derived practical J_{sc} limit is quantified. Based on the magnitude of the gap attributed to specific functional layers, a ranked J_{sc} loss breakdown is presented in Figure 4, wherein the key improvement factors that have the largest magnitude of J_{sc} impact are ranked first. Figure 4 summarizes the simulated J_{sc} gains from the most to the least critical improvement pathways.

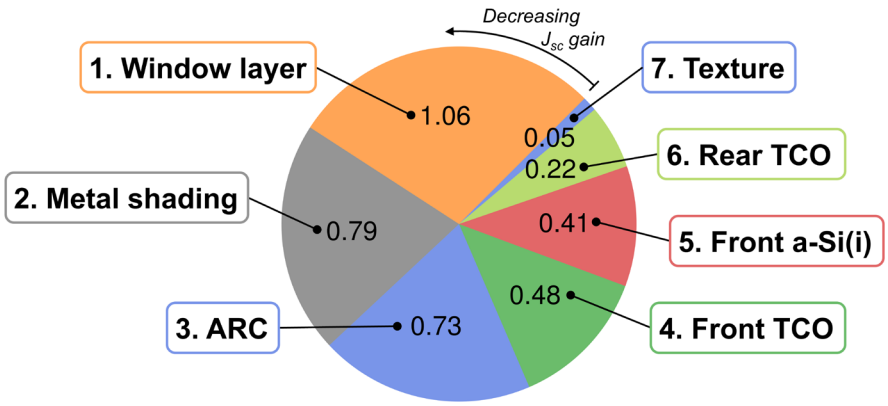

Figure 4. J_{sc} gains in mA/cm^2 for a baseline 37.7 mA/cm^2 FAB SHJ solar cell.

The ranked improvements are as follows:

1. Window layer: Replacing the a-Si:H(n) with more transparent layers (nc-Si:H(n) or nc-SiO_x:H(n)) has the largest impact on J_{sc}.
2. Metal shading: Reducing the front metal fraction from 3.5% to ~1.5% also has a significant impact on the J_{sc}. This low metal fraction can be achieved with either plating or screen printing but is a major challenge currently for screen-printed contacts.
3. ARC: Using a refractive index-matched ARC above the TCO, such as MgF_2 or LiF, leads to a gain in J_{sc}. A further J_{sc} gain is also obtained partly due to the reduction of the optimal thickness of the front TCO for this new bi-layer structure. However, the use of ARC leads to higher cell-to-modules losses, as explained later, thereby making this a less relevant pathway for commercial SHJ solar cells.
4. Front TCO: Replace front ITO with more transparent TCOs such as ICO [18] and IMO [11] has a positive impact on the transparency of the cell over the full spectrum.
5. Front a-Si:H(i): The use of multi-layer a-Si:H(i) films optimized for high transparency (reduced parasitic absorption) but without reducing collection efficiency can improve J_{sc}.
6. Rear TCO: The use of materials similar to the high-transparency front TCO layers but optimized for transparency for wavelengths above 950 nm could improve J_{sc} marginally, although the overall impact is significantly smaller than improvements on the front-side TCOs or other layers.
7. Texture: Improving wafer texturing to reduce the WAR by ~1% (from 13.7% to 12.9%, as measured on a bare textured silicon wafer) has the least impact on J_{sc} and is therefore the least-preferred pathway for J_{sc} improvement.

We comment here in particular on the use of ARC layers, which is a popular method to achieve a quick gain in J_{sc} and has been used to good effect in the recent world-record solar cells. It has to be taken into consideration that the gain in J_{sc} at the cell level cannot be directly translated to gains at the module level; hence, the use of ARCs may not be very relevant for commercial SHJ solar cells. To demonstrate this point, we simulate a SHJ PV module by adding EVA/glass layers in our model (thicknesses of 0.45 mm and 3 mm, respectively) on top of the front TCO of the cell to represent the typical optical structure in a PV module [24-26]. Note that only the active cell area for a single-cell minimodule is considered here. When comparing a SHJ structure with and without a MgF_2 coating, it was observed that adding a MgF_2 ARC results in a net J_{sc} loss of ~0.2 mA/cm^2 at the module level. This is due to the refractive index mismatch between the ARC and the EVA, which leads to a significant increase in front-side reflectance (at the EVA/ARC interface) that offsets the reflectance reduction achieved by the ARC at the cell level. This highlights that the high J_{sc} achieved via ARCs at the cell level is likely not transferrable to the module J_{sc}, which makes ARCs a less viable J_{sc} improvement pathway for commercial SHJ solar cells.

4 Conclusion

In this work, we have investigated the main contributors and pathways to achieving high J_{sc} in FAB SHJ solar cells using a calibrated optical ray-tracing model. We analysed losses in FAB SHJ devices with the highest known J_{sc} values, comparing the loss components for two recent world-record cells and identifying the key improvements necessary to achieve such high J_{sc} performance for “classic” SHJ cells with a-Si:H active layers, ITO-based TCOs and typical screen-printed Ag contacts. The most important improvement pathways were found to be the use of high-transparency window layers, low metal shading (~1.5%) and the inclusion of an ARC. By combining the innovations in the various record solar cells, we estimate the practical J_{sc} limit of FAB SHJ solar cells to be 41.81 mA/cm^2. However, a preliminary analysis of cell-to-module losses suggests that such a high J_{sc} cannot be translated into gains at the PV module level, with ARC layers being particularly ineffective for commercial solar cells and modules.

Appendix A: Optical refractive index data used for record solar cell device modelling (see Figure 5)

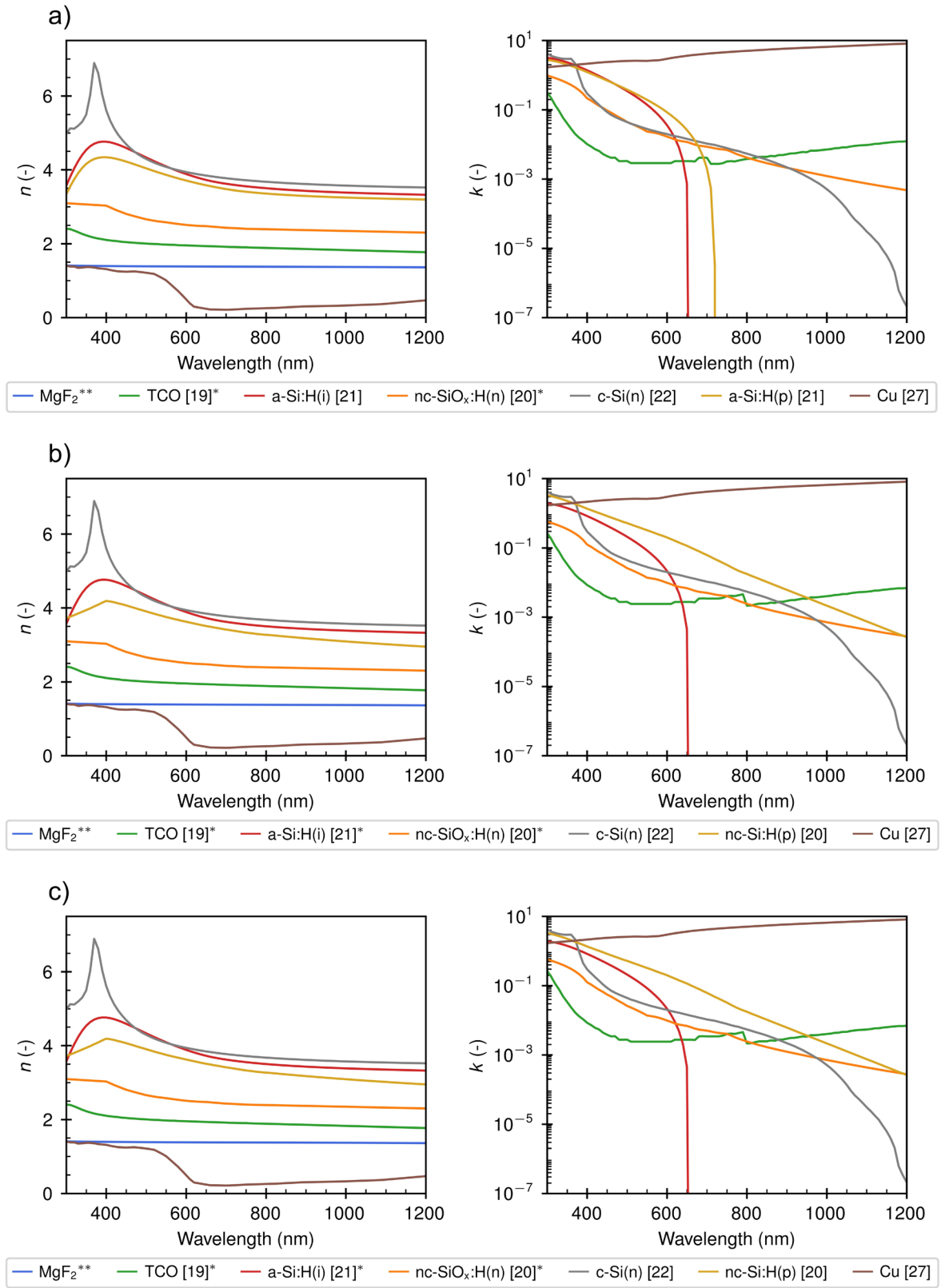

Figure 5. Complex refractive index data of the layers used in the modelled device of a) SunDrive (40.80 mA/cm^2), b) LONGi (41.45 mA/cm^2) and c) the practical limit (41.81 mA/cm^2). The TCO and a-Si:H(i) refractive indices are the same for the front and rear. Notation: (*) literature data has been modified, as explained in the main text, (**) measured in-house.

Appendix B: Adjustment procedure for extinction coefficient (*k*) data

The original data for extinction coefficients for a-Si:H(i), nc-SiO_x:H(n) and TCO are taken from Refs. [21], [20] and [19], respectively. In order to achieve a good fit to the reported EQE and reflectance data of record solar cell devices from SunDrive [9, 11] and LONGi [1], the extinction coefficient (*k*) was multiplied by a scaling factor. In the case of a-Si:H(i) and nc-SiO_x:H(n), a constant scaling factor was applied over the entire wavelength range (300-1200 nm). In the case of TCOs, a different scaling factor was applied to the short-wavelength range and the long-wavelength range. The scaling factors applied are listed in Table 1 and a plot of the original and adjusted data is shown in Figure 6.

Table 1. Scaling factors for complex refractive index data applied to reported data for various thin film layers in order to achieve good fits to reported record solar cells.

Layer	Scaling factor in model for SunDrive record solar cell [9]		Scaling factor in model for LONGi record solar cell [1]		Scaling factor in model for practical J_{sc} limit		Reference data
	n	*k*	*n*	*k*	*n*	*k*	
Front a-Si:H(i)	-	-	-	0.6	-	0.6	[21]
Front nc-SiO_x:H(n)	-	0.6	-	0.35	-	0.35	[20]
Front TCO	-	1.2*, 0.8$^+$	-	0.45$^\#$	-	0.45$^\#$	[19]
Rear a-Si:H(i)	-	-	-	0.6	-	0.6	[21]
Rear a-Si:H(p)/nc-Si:H(p)	-	-	-	-	-	-	[21], [20]
Rear TCO	-	1.2*, 0.8$^+$	-	0.45$^\#$	-	0.45$^\#$	[19]
Copper chuck	-	-	-	-	-	-	[27]

*Applied only to 300-700 nm; $^+$Applied only to 700-1200 nm; $^\#$Applied only to 800-1200 nm.

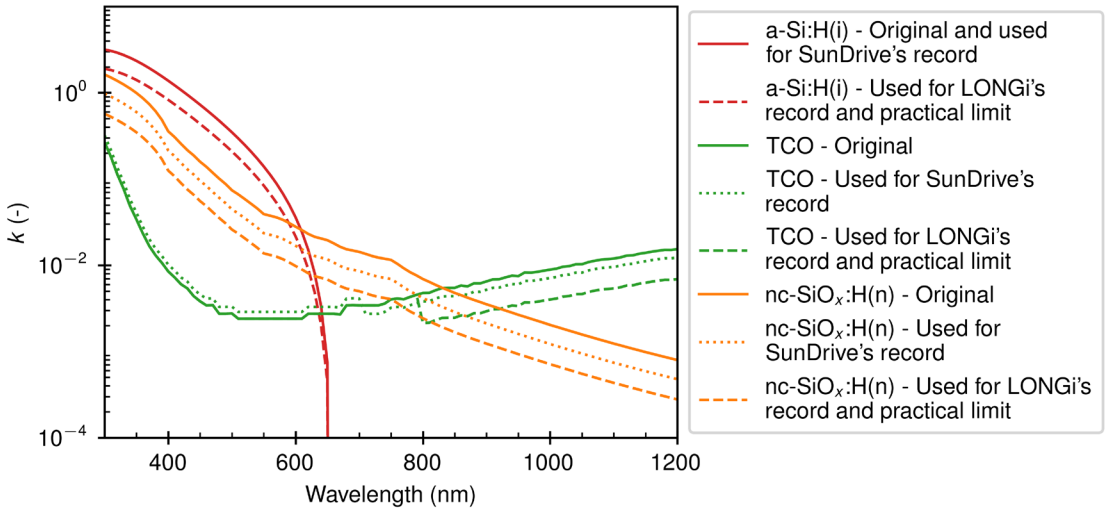

Figure 6. Original and adjusted extinction coefficients *k* for the record devices modelled in Figure 3.

Data availability statement

Reference data for model calibration are found in Refs. [11,18]. Output data from the simulations can be made available upon request.

Author contributions

Erik M. Spaans: Data curation, Formal analysis, Investigation, Methodology, Writing – original draft, review & editing. Selvaraj Venkataraj: Investigation, Resources, Writing – review & editing. Armin G. Aberle: Supervision, Funding acquisition, Writing – review & editing. Nitin Nampalli: Conceptualization, Formal analysis, Project administration, Writing – review & editing.

Competing interests

The authors declare no competing interests.

Funding

This research is supported by the National Research Foundation, Singapore, and the Agency for Science, Technology and Research (A*STAR) under its RIE2020 Industry Alignment Fund – Industry Collaboration Project (IAF-ICP) (Award I1801E0027). SERIS is a research institute at the National University of Singapore (NUS). SERIS is supported by NUS, the National Research Foundation Singapore (NRF), the Energy Market Authority of Singapore (EMA) and the Singapore Economic Development Board (EDB).

Acknowledgement

The authors would like to acknowledge the assistance of Lars Flauger for preliminary measurements on SHJ precursors. We would also like to thank the SERIS project team for fabrication of test samples used for validating the models in this work.

References

1. M. Green et al., "Solar cell efficiency tables (Version 61)," in Prog Photovolt Res Appl., vol. 31, no. 1, pp. 3-16, Jan. 2023, doi: 10.1002/pip.3646.
2. LONGi. “At 26.81%, LONGi sets a new world record efficiency for silicon solar cells.” LONGi News. https://www.longi.com/en/news/propelling-the-transformation/ (accessed Apr. 15, 2023).
3. S. Chunduri. “LONGi creates history by breaking 5-year-old world record silicon solar cell efficiency of Kaneka as it produces 26.81% efficient back contact cell.” Taiyang News. https://taiyangnews.info/technology/longi-breaks-long-time-silicon-solar-cell-record/ (accessed Apr. 15, 2023).
4. LONGi. “LONGi once again sets new world record for HJT solar cell efficiency.” LONGi News. https://www.longi.com/us/news/new-hjt-world-record/ (accessed Apr. 15, 2023).
5. A. Bhambhani. “LONGi’s heterojunction cell efficiency jumps to 26.30% within a week.” Taiyang News. https://taiyangnews.info/technology/26-30-efficiency-for-longis-hjt-solar-cell/ (accessed Apr. 15, 2023).
6. LONGi. “LONGi sets new world record of 25.82% for HJT solar cell efficiency.” LONGi News. https://www.longi.com/en/news/6751/ (accessed Apr. 15, 2023).
7. LONGi. “LONGi breaks three more world records for solar cell efficiency.” LONGi News. https://www.longi.com/en/news/7474/ (accessed Apr. 15, 2023).
8. Aleina. “GS-Solar’s mass produced HJT cell achieves conversion efficiency of 25.2%.” PV Time. https://www.pvtime.org/gs-solars-mass-produced-hjt-cell-achieves-conversion-efficiency-of-25-2/ (accessed Apr. 15, 2023).
9. D. Carrol. “SunDrive achieves 26.41% efficiency with copper-based solar cell tech.” PV Magazine. https://www.pv-magazine.com/2022/09/05/sundrive-achieves-26-41-efficiency-with-copper-based-solar-cell-tech/ (accessed Apr. 15, 2023).

10. D. Carrol. “SunDrive sets 26.07% efficiency record for heterojunction PV cell in mass production.” PV Magazine. https://www.pv-magazine.com/2022/03/17/sundrive-sets-26-07-efficiency-record-for-heterojunction-pv-cell-in-mass-production/ (accessed Apr. 15, 2023).
11. T. Tang et al., "Achievement of 25.54% power conversion efficiency by optimization of current losses at the front side of silicon heterojunction solar cells," in Prog Photovolt Res Appl, vol. 31, no. 5, pp. 449-460, May 2023, doi: 10.1002/pip.3641.
12. E. Bellini. “Huasun achieves 25.26% efficiency for heterojunction solar cell.” PV Magazine. https://www.pv-magazine.com/2021/07/13/huasun-achieves-25-26-efficiency-for-heterojunction-solar-cell/ (accessed Apr. 15, 2023).
13. A. Bhambhani. “Tested By ISFH Germany, Chinese heterojunction cell & module producer Huasun energy reports 25.23% efficiency for 166mm wafer sized HJT cell.” Taiyang News. https://taiyangnews.info/technology/25-23-conversion-efficiency-for-huasuns-hjt-solar-cell/ (accessed Apr. 15, 2023).
14. M. Hutchins. “Hanergy hits 25.11% efficiency with HJT cell.” PV Magazine. https://www.pv-magazine.com/2019/11/20/hanergy-sets-new-heterojunction-module-efficiency-record/ (accessed Apr. 15, 2023).
15. A. Bhambhani. “Suzhou Maxwell scores 25.62% efficiency using low indium & silver coated copper grid lines.” Taiyang News. https://taiyangnews.info/technology/25-62-efficiency-for-silicon-hjt-cell/ (accessed Apr. 15, 2023).
16. R. Santbergen, T. Meguro, T. Suezaki, G. Koizumi, K. Yamamoto and M. Zeman, "GenPro4 optical model for solar cell simulation and its application to multijunction solar cells," in IEEE Journal of Photovoltaics, vol. 7, no. 3, pp. 919-926, May 2017, doi: 10.1109/JPHOTOV.2017.2669640.
17. Z. C. Holman et al., "Current losses at the front of silicon heterojunction solar cells," in IEEE Journal of Photovoltaics, vol. 2, no. 1, pp. 7-15, Jan. 2012, doi: 10.1109/JPHOTOV.2011.2174967.
18. H. Lin et al., "26.7% efficiency silicon heterojunction solar cells achieved by electrically optimized nanocrystalline-silicon hole contact layers," Preprint, Jan. 2023, doi: 10.21203/rs.3.rs-2402141/v1.
19. S. An et al., "Cerium-doped indium oxide transparent electrode for semi-transparent perovskite and perovskite/silicon tandem solar cells," in Solar Energy, vol. 196, pp. 409-418, Jan. 2020, doi: 10.1016/j.solener.2019.12.040.
20. S. Abolmasov, P. R. i Cabarrocas and P Chatterjee, "Towards 12% stabilised efficiency in single junction polymorphous silicon solar cells: experimental developments and model predictions," in EPJ Photovoltaics, vol. 7, Jan. 2016, doi: 10.1051/epjpv/2015011.
21. M. Leilaeioun, “Intrinsic amorphous silicon deposited by PECVD”, Unpublished (2018).
22. M. Green, "Self-consistent optical parameters of intrinsic silicon at 300 K including temperature coefficients," in Solar Energy Materials and Solar Cells, vol. 92, no. 11, pp. 1305-1310, Nov. 2008, doi: 10.1016/j.solmat.2008.06.009.
23. A. Bhambhani. “Maxwell & SunDrive further improve silver free HJT cell efficiency to 26.41%, inching towards global silicon cell record.” Taiyang News. https://taiyangnews.info/technology/impressive-26-41-hjt-solar-cell-efficiency/ (accessed Apr. 15, 2023).
24. K. R. McIntosh, J. N. Cotsell, J. S. Cumpston, A. W. Norris, N. E. Powell and B. M. Ketola, "An optical comparison of silicone and EVA encapsulants for conventional silicon PV modules: A ray-tracing study," 2009 34th IEEE Photovoltaic Specialists Conference (PVSC), Philadelphia, PA, USA, 2009, pp. 000544-000549, doi: 10.1109/PVSC.2009.5411624.
25. M. R. Vogt et al., "Measurement of the optical constants of soda-lime glasses in dependence of iron content and modeling of iron-related power losses in crystalline Si solar cell modules," in IEEE Journal of Photovoltaics, vol. 6, no. 1, pp. 111-118, Jan. 2016, doi: 10.1109/JPHOTOV.2015.2498043.
26. M. R. Vogt et al., "Optical constants of UV transparent EVA and the impact on the PV module output power under realistic irradiation," in Energy Procedia, vol. 92, pp. 523-530, Aug. 2016, doi: 10.1016/j.egypro.2016.07.136.

27. P. B. Johnson and R. W. Christy, "Optical constants of the noble metals," in Phys. Rev. B, vol. 6, no. 12, pp. 4370-4379, Dec. 1972, doi: 10.1103/PhysRevB.6.4370.